Multidimensional scattering of attosecond x-ray pulses detected by photon-coincidence

2014 J. Phys. B: At. Mol. Opt. Phys. 47 124037

(http://iopscience.iop.org/0953-4075/47/12/124037)

IOP Publishing Journal of Physics B: Atomic, Molecular and Optical Physics

J. Phys. B: At. Mol. Opt. Phys. **47** (2014) 124037 (8pp) doi:10.1088/0953-4075/47/12/124037

Multidimensional scattering of attosecond x-ray pulses detected by photon-coincidence

Jason D Biggs, Kochise Bennett, Yu Zhang and Shaul Mukamel

University of California, Irvine, CA 92697-2025, USA

E-mail: biggsj@uci.edu, kcbennet@uci.edu, yuz10@uci.edu and smukamel@uci.edu

Received 5 December 2013, revised 10 February 2014
Accepted for publication 7 March 2014
Published 10 June 2014

Abstract

We propose a new photon-coincidence measurement based on the time- and wavevector-resolved detection of photons generated by the scattering of multiple x-ray pulses with variable delays. The technique directly measures multipoint correlation functions of the charge density through superpositions of valence excitations which are created impulsively by the scattering process.

Keywords: x-ray, attosecond, scattering

(Some figures may appear in colour only in the online journal)

1. Introduction

Experiments which employ sequences of attosecond pulses to probe the electronic and nuclear dynamics of molecules in the condensed phase with sub-femtosecond time and atomic spatial resolution are made possible by newly developed bright sources of soft and hard x-ray light [1–6]. These techniques provide novel windows into molecular valence electronic structure and chemical dynamics with much higher resolution than is possible with visible light. Valence-electron motions can be triggered impulsively by core excitations and then monitored by x-ray pulse sequences. Coherent stimulated x-ray Raman signals (SXRS), which observe electron wavepackets created by attosecond pulses, may be described by extending concepts used for vibrational wavepackets in the visible regime [7]. The pulse envelopes in these time-domain analogues of resonant inelastic x-ray scattering allow to control both excitation and observation windows. Multidimensional time-resolved photoelectron signals are possible as well, and the quantum properties of the x-ray fields can be exploited to control pathways in matter [8].

Resonant x-ray scattering is spatially selective and can create a perturbation of the electronic charge distribution in the vicinity of a selected atom [9]. Off-resonant scattering is not spatially selective but offers a new window through the wavevector dependence of the signal. If a scattering event of a $\mathbf{k}_1$ photon is recorded at time T_1 with scattering wavevector $\mathbf{k}_1$ then we know that it leaves the molecule in the superposition of valence electronic eigenstates $\hat{\sigma}(\mathbf{q}_1)|g\rangle$, where $\hat{\sigma}$ is the electronic charge-density operator in the many-electron space and the scattering wavevector $\mathbf{q}_1 = \mathbf{k}_1 - \mathbf{k}_I$ is the difference between incoming and outgoing wavevectors. If at time T_2 we then record the scattering of a $\mathbf{k}_2$ photon this event amplitude is given by a projection of that evolving superposition onto the subspace defined by the operator $\hat{\sigma}(\mathbf{q}_2)$. Each $\mathbf{k}_1$ and $\mathbf{k}_2$ pair represents a separate window into the time evolution of the electronic wavepacket.

One exciting application of x-ray free electron laser sources is the possible determination of electronic structure by x-ray diffraction of single molecules, eliminating the tedious and often prohibitively time-consuming requirement to crystalize samples such as proteins [10, 11]. It follows from our recent work on spontaneous emission of visible photons following impulsive x-ray Raman excitation [12] that inelastic scattering, which does not contribute for Bragg diffraction, is more pronounced for single molecules.

Diffraction is usually calculated by treating the x-ray field as classical. The signal depends solely on the time-dependent charge density. In a quantum description of the field [13, 14], the off-resonant x-ray scattering signal has both an elastic (Thomson or Rayleigh) and an inelastic (Compton or Raman-type) components. Only the former is related to the charge

density and may be used to obtain the electronic structure of a crystal. The latter involves a radiation back-reaction that is missed by the classical treatment, and depends on transition amplitudes between valence excitations. We have developed a quantum-field treatment of x-ray scattering [15]. Extending that analysis to a molecule initially prepared in an electronic superposition state [16–19] will make it possible to track the time-dependent electron density.

Multidimensional nonlinear spectroscopy is a class of techniques in which multiple pulses are directed at the sample and the intensity change of one of the beams is detected. By varying the time delays between these pulses, as well as other parameters (e.g. frequencies, polarizations, phases), multidimensional plots can be constructed and the resulting pattern of peaks reveal resonances in the material [20]. In this paper, we propose to generate multidimensional signals by using off-resonant scattering of two or more shaped broadband x-ray pulses. This permits the probing of correlations in electronic structure at different times controlled by the scattered pulses [21]. Throughout, we define the signal as the intensity of the gated x-ray electric field [12]. A variety of different detection modes are possible. Importantly, the proposed technique requires single-photon detection (photon $\mathbf{k}_1$ is scattered at T_1, photon $\mathbf{k}_2$ at T_2, etc) so that the state of the system following each scattering event is well controlled. We demonstrate that these techniques provide valuable information about nonlinear charge fluctuations in molecules.

Thanks to their broad spectral bandwidth, short pulses can induce transitions between many-electron states of the molecule which generate the signal. Due to the coherences induced by the scattered x-ray pulses, the signal is not simply given by the momentum space charge-density or a correlation function thereof. Given the plethora of parameter choices for such techniques, it is likely that they will be useful as a complement to the ordinary (one-dimensional) x-ray scattering signal.

2. Multidimensional scattering off a single particle

2.1. Correlation function expressions

We begin by reviewing the resonant x-ray scattering technique SXRS. In that case, the interaction Hamiltonian is written

$$\hat{H}'(t) = \frac{e}{c}\hat{\mathbf{p}}\cdot\hat{\mathbf{A}}(t) \tag{1}$$

where $\mathbf{p}$ and $\mathbf{A}(t)$ are the momentum and vector potential, respectively. In an SXRS process, a valence excitation results from two successive field-matter interactions via a high-energy core-excited intermediate state. The broad bandwidth of attosecond pulses creates a superposition of such valence excited states, and by tuning the pulse to be resonant with a given core edge, this electronic wavepacket is initially localized near that core orbital.

Resonant x-ray spectroscopies probe the multipoint correlation functions of the dipole operator between the core and valence levels [20, 22]. SXRS, in contrast, depends on correlation functions of the broadband core polarizability $\hat{\alpha}$,

$$\hat{\alpha} = \sum_{c,e,e'} |e\rangle \frac{(\boldsymbol{\epsilon}_R\cdot\boldsymbol{\mu}_{ec})(\boldsymbol{\epsilon}_R\cdot\boldsymbol{\mu}_{ce'})}{2\pi} \times \int_{-\infty}^{\infty} \mathrm{d}\omega \frac{\hat{\mathcal{A}}_R^*(\omega)\hat{\mathcal{A}}_R(\omega+\omega_{ee'})}{\omega-\omega_{ce}+i\Gamma_c}\langle e'|. \tag{2}$$

Here $\hat{\mathcal{A}}_R(\omega)$ and $\boldsymbol{\epsilon}_R$ are the envelope and polarization vector for the Raman pulse, $\boldsymbol{\mu}_{ec}$ and ω_{ce} are the transition frequency and dipole matrix element between core excited state c and valence state e, and Γ_c is the inverse core-hole lifetime. One-dimensional SXRS is a two-pulse experiment with a single delay period T, and is associated with the correlation function

$$S(T) \propto \langle\hat{\alpha}(T)\hat{\alpha}(0)\rangle - \langle\hat{\alpha}^\dagger(0)\hat{\alpha}(T)\rangle \tag{3}$$

where $\langle x\rangle \equiv \mathrm{Tr}[x\rho]$, and the operators are written in the interaction picture. In this section, we assume that the system is initially in the electronic ground state, such that at time 0 we have $\rho = |g\rangle\langle g|$. This assumption is relaxed in the next section. Two-dimensional SXRS uses three pulses, depends on two time delays, and is associated with [7]

$$S(T_1,T_2) \propto \langle\hat{\alpha}(T_1+T_2)\hat{\alpha}(T_1)\hat{\alpha}(0)\rangle - \langle\hat{\alpha}^\dagger(0)\hat{\alpha}(T_1+T_2)\hat{\alpha}(T_1) + \langle\hat{\alpha}^\dagger(0)\hat{\alpha}^\dagger(T_1)\hat{\alpha}(T_1+T_2)\rangle - \langle\hat{\alpha}^\dagger(T_1)\hat{\alpha}(T_1+T_2)\hat{\alpha}(0)\rangle. \tag{4}$$

Equation (1) applies below and slightly above the various ionization-edges of the atoms in the system. Off-resonant scattering, where photon energies are far above any of the ionization thresholds, is determined by the following radiation-matter interaction Hamiltonian

$$\hat{H}'(t) = \int \mathrm{d}\mathbf{r}\hat{\mathbf{A}}^2(\mathbf{r},t)\hat{\sigma}(\mathbf{r},t), \tag{5}$$

where the charge density operator $\hat{\sigma}(\mathbf{r},\mathbf{t})$ written in the interaction picture is related by a spatial Fourier transform to $\sigma(\hat{\mathbf{q}},t)$.

One example of a time-dependent scattering signal involves two x-ray pulses with a single time delay, making it a one-dimensional signal. The first pulse, arriving at time 0, is resonant with a core-to-valence transition and its interaction is governed by equation (1). The second pulse, arriving at time T, is off resonance and interacts with the system via equation (5). The correlation function for this signal is

$$S(\mathbf{k}_1,T) \propto \langle\hat{\sigma}^\dagger(T,\mathbf{q}_1)\hat{\sigma}(T,\mathbf{q}_1)\hat{\alpha}(0)\rangle - \langle\hat{\alpha}^\dagger(0)\hat{\sigma}^\dagger(T,\mathbf{q}_1)\hat{\sigma}(T,\mathbf{q}_1)\rangle. \tag{6}$$

This is a simplified expression, showing only the underlying correlation function. The full expression is given by equation (8) of [15] where we also present simulations for the amino acid cysteine at the sulfur K-edge.

The scattering signal will, in general, contain both elastic and inelastic scattering contributions. Since the core polarizability acts only on one side of the density matrix (in the first and second terms of the right-hand side of equation (6), $\hat{\alpha}$ acts on the ket and bra, respectively), the system is prepared in an electronic coherence rather than a population. In this case, elastic scattering will only occur from that portion of the electronic wavefunction still in the ground state, and will

give a delay-time-independent background. By isolating the portion of the scattering signal that changes with T, we can eliminate the elastic-scattering contribution.

The signals described so far do not require single-photon counting, and can be carried out using strong fields. Signals which probe correlation functions of the charge density will be experimentally more challenging. In the simplest such experiment, a single molecule is subjected to two attosecond off-resonant pulses, with wavevectors $\mathbf{k}_I$ and $\mathbf{k}_{II}$. A single scattered photon with frequency ω_1 from pulse I is collected in the direction $\mathbf{k}_1$ at time 0, and the molecule is left in a superposition state for the interpulse delay, after which the second pulse is scattered, and photons of frequency ω_2 are collected in a variety of directions $\mathbf{k}_2$ at time T.

The signal that results from two successive scattering measurements is determined by the correlation function

$$S(\mathbf{k}_1, \mathbf{k}_2, T) \propto \langle \hat{\sigma}^\dagger(0, \mathbf{q}_1)\hat{\sigma}^\dagger(T, \mathbf{q}_2)\hat{\sigma}(T, \mathbf{q}_2)\hat{\sigma}(0, \mathbf{q}_1)\rangle. \quad (7)$$

This signal is one-dimensional in that it only depends on a single time delay T. Two-dimensional signals are acquired by the application of one Raman and two scattering pulses

$$\begin{aligned} S(\mathbf{k}_1, T_1, \mathbf{k}_2, T_2) \propto & \langle \hat{\sigma}^\dagger(T_1, \mathbf{q}_1)\hat{\sigma}^\dagger(T_1+T_2, \mathbf{q}_2) \\ & \times \hat{\sigma}(T_1+T_2, \mathbf{q}_2)\hat{\sigma}(T_1, \mathbf{q}_1)\hat{\alpha}(0)\rangle \\ & - \langle \hat{\alpha}^\dagger(0)\hat{\sigma}^\dagger(T_1, \mathbf{q}_1)\hat{\sigma}^\dagger(T_1+T_2, \mathbf{q}_2) \\ & \times \hat{\sigma}(T_1+T_2, \mathbf{q}_2)\hat{\sigma}(T_1, \mathbf{q}_1)\rangle, \end{aligned} \quad (8)$$

or by three successive scattering measurements

$$\begin{aligned} S(\mathbf{k}_1, \mathbf{k}_2, T_2, \mathbf{k}_3, T_3) \propto & \langle \hat{\sigma}^\dagger(0, \mathbf{q}_1)\hat{\sigma}^\dagger(T_1, \mathbf{q}_2) \\ & \times \hat{\sigma}^\dagger(T_1+T_2, \mathbf{q}_3)\hat{\sigma}(T_1+T_2, \mathbf{q}_3)\hat{\sigma}(T_1, \mathbf{q}_2)\hat{\sigma}(0, \mathbf{q}_1)\rangle. \end{aligned} \quad (9)$$

The equations above show how we can describe different x-ray experiments, with combinations of resonant and off-resonant pulses, using a common framework. Both resonant Raman and off-resonant scattering interactions will leave the molecule in an electronic superposition state. Even though the light-matter interactions are different in these cases, the response-function approach results in very similar expressions. In [15] we examined the Raman/scattering signal described by equation (6). In this paper, we look at the two-photon coincidence measurement, equation (7).

2.2. Signal expressions

We consider experiments in which a series of pulses are scattered by a single molecule. The pulses can have arbitrary spectral and temporal shape, provided they are non-overlapping in time and far from any material resonance. Under these conditions the field-matter interaction Hamiltonian is given by equation (5). Such experiments have been proposed as a means of taking stroboscopic images of systems in non-equilibrium states and thus tracking the system's evolution [23–26]. The use of temporally well-separated pulses reflects the experimental goal of taking 'pictures' of the system at distinct points in time and creating a stop-motion style recording and, furthermore, greatly simplifies the resulting expressions. The proposed experiment must involve single-photon coincidence counting; otherwise information about the

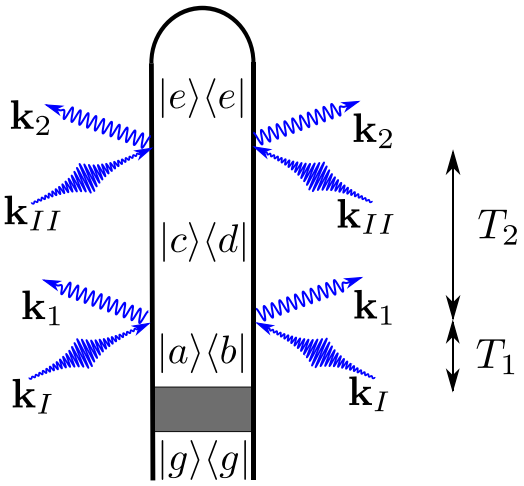

Figure 1. Loop diagram for two-dimensional, off resonant x-ray scattering from a single particle. The particle is initially in its ground state $|g\rangle$ after which, an unspecified process (represented by a shaded box) prepares it in a superposition state. Two well-separated pulses then sequentially scatter from the sample and are detected by a pixel array. The delays T_1 and T_2 can be independently varied.

dependence of the signal on both $\mathbf{k}_1$ and $\mathbf{k}_2$ is averaged out across the diffraction pattern.

The manipulations employed in the derivation of single-dimensional x-ray scattering are valid for each diffraction event separately and the results from [15] are straightforwardly generalized. Figure 1 shows a loop diagram representation of the signal described here. These diagrams [27], show the state-space pathways that lead to a measurement. The left and right branches of the loop represent the ket and bra and real time flows from bottom (initial state) to top (measurement event). We can read off the diffraction signal from figure 1 as

$$\begin{aligned} S(\mathbf{k}_1, T_1, \mathbf{k}_2, T_2) = & \sum_{abcde} \rho_{ab}\omega_1^2\omega_2^2\mathcal{A}_I(\omega_1+\omega_{ca})\mathcal{A}_I^*(\omega_1+\omega_{db}) \\ & \times \mathcal{A}_{II}(\omega_2+\omega_{ec})\mathcal{A}_{II}^*(\omega_2+\omega_{ed})\sigma_{ca}\left(\mathbf{q}_{ca}^{(1)}\right) \\ & \times \sigma_{db}^*\left(\mathbf{q}_{db}^{(1)}\right)\sigma_{ec}\left(\mathbf{q}_{ec}^{(2)}\right)\sigma_{ed}^*\left(\mathbf{q}_{ed}^{(2)}\right)\mathrm{e}^{-\mathrm{i}(\omega_{ab}T_1+\omega_{cd}T_2)}. \end{aligned} \quad (10)$$

In this expression, $\mathcal{A}_I$ ($\mathcal{A}_{II}$) is the spectral envelope for the first (second) pulse, a, b, c, d, and e represent valence eigenstates of the material Hamiltonian and ω_1 (ω_2) are the first (second) detected frequencies. Equation (10) includes matrix elements σ_{ij} of the charge density operator in the basis of electronic eigenstates of the molecule. The time between the initial state preparation and the centre of the first diffracting pulse is labelled T_1 and the time between the two diffracting pulses is labelled T_2. Finally, the scattering vectors are defined by $\mathbf{q}_{ab}^{(1(2))} \equiv \mathbf{k}_{1(2)} - \frac{\omega_{1(2)}+\omega_{ab}}{c}\hat{\mathbf{k}}_{I(II)}$ where $\hat{\mathbf{k}}_I$ ($\hat{\mathbf{k}}_{II}$) is the wavevector of the first (second) pulse.

When the system is initially in a pure state (i.e. $\rho_{ab} = c_a c_b^*$ where c_a, c_b are the amplitudes of state a, b so that the state of the system is $|\psi\rangle = \sum_a c_a|a\rangle$), equation (10) can be recast into a Kramers–Heisenberg (modulus square) form

$$\begin{aligned} S(\mathbf{k}_1, T_1, \mathbf{k}_2, T_2) = & \sum_e \left| \sum_{ac} c_a\omega_1\omega_2\mathcal{A}_I(\omega_1+\omega_{ca}) \right. \\ & \left. \times \mathcal{A}_{II}(\omega_2+\omega_{ec})\sigma_{ca}(\mathbf{q}_{ca}^{(1)})\sigma_{ec}(\mathbf{q}_{ec}^{(2)})\mathrm{e}^{-\mathrm{i}\left(\omega_{ae}T_1+\omega_{ce}T_2\right)} \right|^2. \end{aligned} \quad (11)$$

In many situations it is not feasible to calculate the electronic eigenstates of the system, and it is therefore desirable to rewrite equation (10) in terms of a time-correlation function of the charge density. By assuming a flat pulse-envelope (i.e. the spectral pulse envelopes are uniform over the range of material eigenenergies so that $\mathcal{A}_{I/II}(\omega_{1/2} - \omega_{ab}) \approx \mathcal{A}_{I/II}(\omega_{1/2})$ for any material states a, b), we recast equation (10) as

$$S(\mathbf{k}_1, T_1, \mathbf{k}_2, T_2) = |\omega_1\omega_2\mathcal{A}_I(\omega_1)\mathcal{A}_{II}(\omega_2)|^2 \times \int \mathrm{d}\mathbf{r}\mathrm{d}\mathbf{r}'\mathrm{d}\mathbf{r}''\mathrm{d}\mathbf{r}'''\mathrm{e}^{-\mathrm{i}\mathbf{q}^{(1)}\cdot(\mathbf{r}-\mathbf{r}''')}\mathrm{e}^{-\mathrm{i}\mathbf{q}^{(2)}\cdot(\mathbf{r}'-\mathbf{r}'')} \times\langle\hat{\sigma}^\dagger(\mathbf{r}''', T_1 + \hat{\mathbf{k}}_I\cdot\mathbf{r}'''/c)\hat{\sigma}^\dagger(\mathbf{r}'', T_1 + T_2 + \hat{\mathbf{k}}_{II}\cdot\mathbf{r}''/c) \times\hat{\sigma}(\mathbf{r}', T_1 + T_2 + \hat{\mathbf{k}}_{II}\cdot\mathbf{r}'/c)\hat{\sigma}(\mathbf{r}, T_1 + \hat{\mathbf{k}}_I\cdot\mathbf{r}/c)\rangle. \quad (12)$$

This expression incorporates the effect of inelastic scattering on the momentum transfer, but does not hold for arbitrarily shaped pulses. Equation (12) is simplified when considering only elastic scattering, yielding

$$S(\mathbf{k}_1, T_1, \mathbf{k}_2, T_2) = |\omega_1\omega_2\mathcal{A}_I(\omega_1)\mathcal{A}_{II}(\omega_2)|^2\langle\hat{\sigma}^\dagger\left(\mathbf{q}_0^{(1)}, T_1\right) \times\hat{\sigma}^\dagger\left(\mathbf{q}_0^{(2)}, T_1 + T_2\right)\hat{\sigma}\left(\mathbf{q}_0^{(2)}, T_1 + T_2\right)\hat{\sigma}\left(\mathbf{q}_0^{(1)}, T_1\right)\rangle \quad (13)$$

with $\mathbf{q}_0^{(1(2))} \equiv \mathbf{q}_{aa}^{(1(2))}$ as the elastic scattering vector.

3. Simulations

3.1. Electronic structure

We have simulated the two-photon coincident measurement on the sulfur-containing amino acid cysteine. Cysteine affects protein structure because of the disulfide bonds it forms. We have previously explored various resonant x-ray spectroscopic signals from this molecule, including SXRS and x-ray photon echo [22, 28]. Details of the electronic structure calculations can be found in [28], and are recounted briefly here. The optimized geometry of cysteine was obtained with the Gaussian09 package [29] at the B3LYP [30, 31]/6-311G** level of theory. Valence-excited states were found at the CAM-B3LYP [32]/6-311G** level of theory, and with the Tamm–Dancoff approximation [33] using a locally modified version of NWChem [34, 35].

Since the higher-order energy gradient TDDFT is not available in the current code, transition density matrices between different valence excited states, which contribute to the summation in equation (9), are calculated using the CI coefficients from the TDDFT results, and are therefore an unrelaxed excited-state property. For higher accuracy, we should calculate such relaxed excited state properties using the Z-vector method [36, 37]. This is left for future studies.

3.2. One-dimensional signals: two scattering events

We first examine the scattering signal from the ground state. The states a and b in figure 1 and equation (10) are set equal to the ground state g. In this case, we can recast the signal as a modulus square of an amplitude

$$S(\mathbf{k}_1, \mathbf{k}_2, T) = \left|\sum_{ce}\omega_1\omega_2\mathcal{A}_I(\omega_1 + \omega_{cg})\mathcal{A}_{II}(\omega_2 + \omega_{ec}) \times\sigma_{cg}\left(\mathbf{q}_{cg}^{(1)}\right)\sigma_{ec}\left(\mathbf{q}_{ec}^{(2)}\right)\mathrm{e}^{-\mathrm{i}\epsilon_c T_2}\right|^2. \quad (14)$$

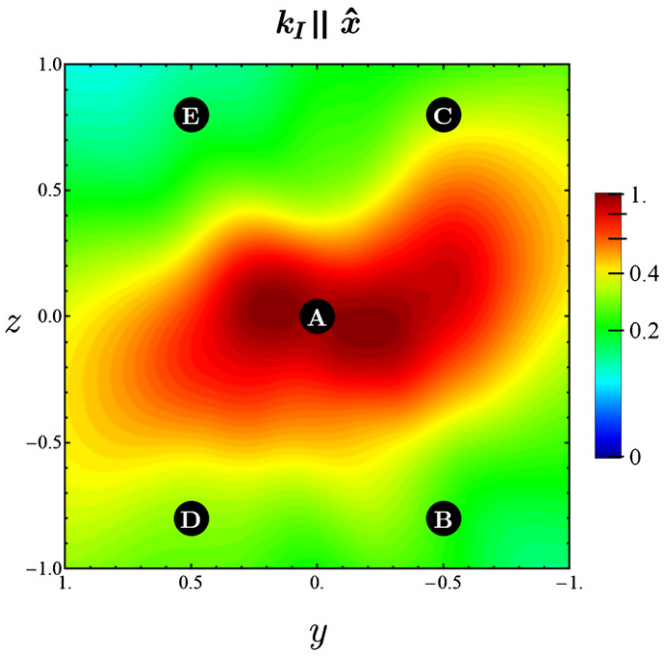

Figure 2. Ground-state scattering pattern for cysteine with $\mathbf{k}_I$ set along the lab-frame x-axis, and the detection frequency ω_1 set to the pulse central frequency. Four peaks are chosen in the $\mathbf{k}_I$ pattern. The spatial orientation of the molecule with respect to the incoming wavevectors is shown in figure 3.

We took the sample to be a single cysteine molecule oriented in the lab frame. The transform-limited Gaussian pulse has a central frequency of 10 keV and a duration of 500 as FWHM (3.65 as FWHM). The scattered photons are collected on a square grid 2 cm in length positioned 1 cm from the molecule. We take the wavevector for the first pulse to be along the lab-frame x-axis. Figure 2 shows the single-pulse scattering signal. For the coincidence measurement, we wish to eliminate the elastic contribution, where state c in equation (14) is the ground state g, which is independent of the delay T. To this end, we take the detected frequency for the first photon to be $\omega_1 = \Omega_I - 8\,\mathrm{eV}$, ensuring that only states whose excitation energies ω_{cg} are within a region around 8 eV defined by the pulse bandwidth contribute to the signal. Our simulations include fifty valence-excited states with energies between 5 and 11 eV, all of which fit this criterion. The frequency of the second photon was taken to be $\omega_2 = \Omega_{II} + 8\,\mathrm{eV}$, preferentially detecting scattering events where the system returns to the ground state after interaction.

We selected five peaks from the $\mathbf{k}_1$ signal, taken with ω_1 equal to the pulse central frequency Ω_I, and look at the differences in the $\mathbf{k}_2$ pattern for these points. Figure 3 shows an example of a $\mathbf{k}_2$ scattering pattern when $\mathbf{k}_1$ is taken to be peak A. figure 4 shows isosurfaces of the charge density for the molecule following the measurement of photon $\mathbf{k}_1$ for the five labelled peaks in figure 2. The density is defined by

$$\langle\sigma(\mathbf{r}, T)\rangle = \sum_{cd}\mathcal{A}_I(\omega_1 + \omega_{cg})\mathcal{A}_I^*(\omega_1 + \omega_{dg})\sigma_{dg}^*\left(\mathbf{q}_{dg}^{(1)}\right) \times\sigma_{dc}(\mathbf{r})\sigma_{cg}\left(\mathbf{q}_{cg}^{(1)}\right)\mathrm{e}^{-\mathrm{i}\omega_{cd}T}. \quad (15)$$

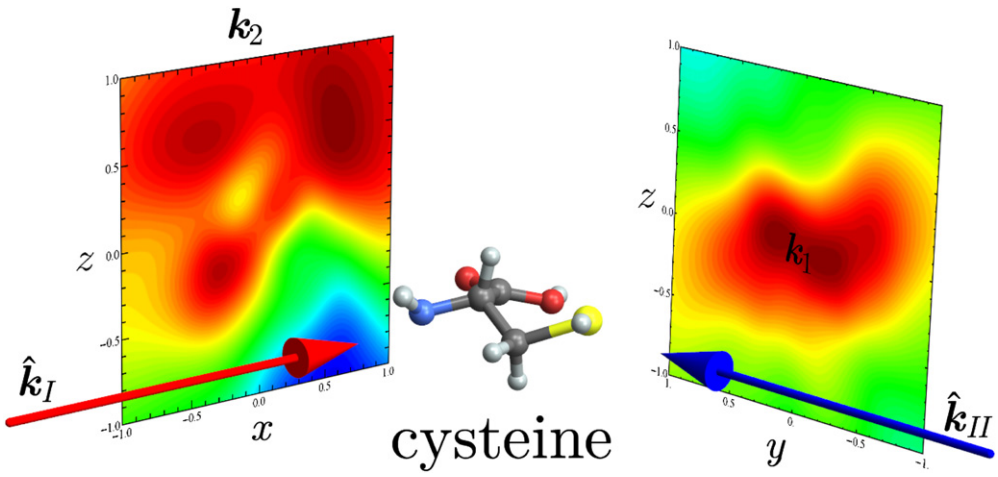

Figure 3. Two-photon coincidence measurement for the molecule cysteine. We show the wavevector for the first pulse $\mathbf{k}_I$ in red, and for the second pulse $\mathbf{k}_{II}$ in blue. $\mathbf{k}_I$ and $\mathbf{k}_{II}$ are aligned with the lab frame x and y axes, respectively, and the orientation of the molecule is shown in the middle. The panel to the right shows the $\mathbf{k}_1$ scattering pattern from figure 2. In a coincidence measurement only a single $\mathbf{k}_1$ photon is detected, leaving the molecule in a superposition state. The $\mathbf{k}_2$ scattering pattern on the left corresponds to detecting a single photon $\mathbf{k}_1$ at the point indicated on the right panel.

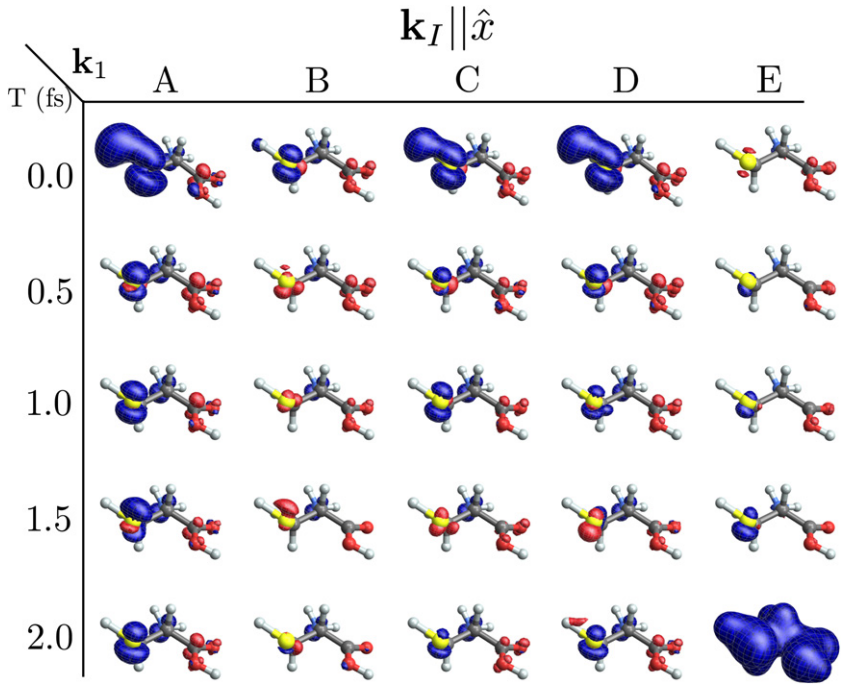

Figure 4. Time dependent charge density (equation (15)) of cysteine after detection of a scattered $\mathbf{k}_1$ photon detected at one of the five points labelled in figure 2. We show the full density only for peak E at $T = 2$ fs, and all other plots have this density subtracted to highlight the changes.

For the reasons described below, the densities for the different peaks and times look very similar. To highlight the differences, in figure 4 we plot the density differences, with the peak E $T = 2$ fs subtracted prior to plotting. We see that the initial density, for $T = 0$ fs is very similar for peaks A, C, and D, and is different for peaks B and E. However, it is difficult to see differences in the charge density at later times. This is due to the fact that the dominant terms in equation (15) occur when states c and d are the same, and do not depend on the delay time. These involve diagonal elements of the charge density $\sigma_{cc}(\mathbf{r})$, which are much larger than off-diagonal elements. In the scattering signals we are able to eliminate such terms, which are independent of the interpulse delay, by choosing the detection frequency to be outside the pulse bandwidth.

Figure 5 shows the $\mathbf{k}_2$ scattering pattern when both $\mathbf{k}_I$ and $\mathbf{k}_{II}$ are set parallel to the x-axis. As can be seen from the top row, wherein the interpulse delay T is set to zero, the $\mathbf{k}_2$ scattering pattern strongly varies with $\mathbf{k}_1$. The choice of $\mathbf{k}_1$ determines the nature of the electronic superposition that is measured in the second scattering event. The first measurement leaves the molecule in a superposition state because it is the photon, not the molecule, that is measured. By detecting photon $\mathbf{k}_1$, we

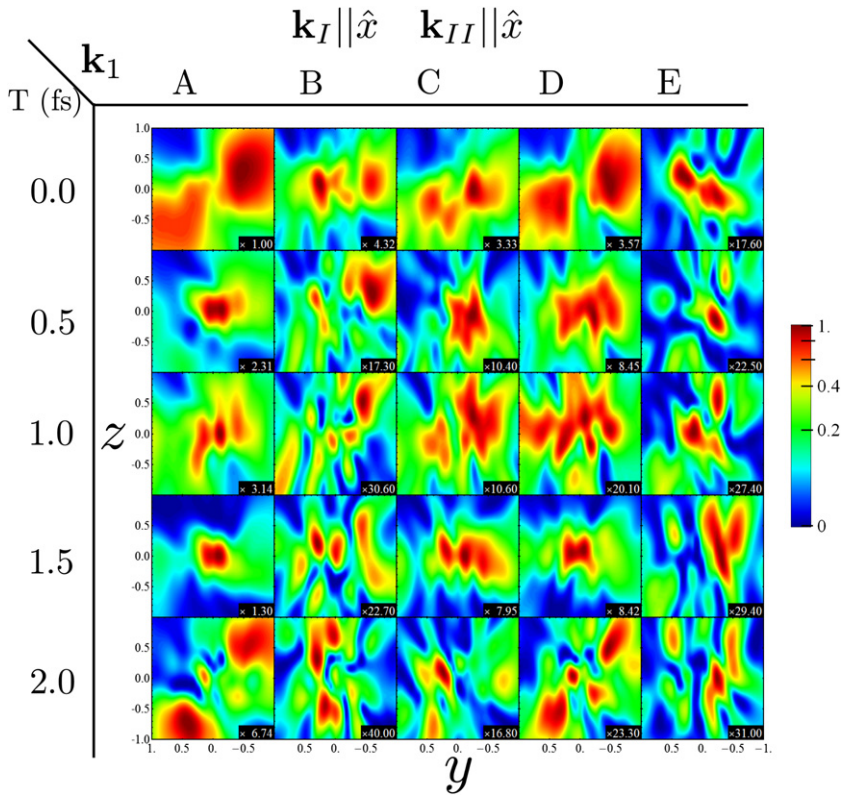

Figure 5. Two-photon coincidence $\mathbf{k}_2$ scattering patterns for five different interpulse delays. $\mathbf{k}_I$ and $\mathbf{k}_{II}$ are both set to the lab-frame x-axis, with $\mathbf{k}_1$ taken to be one of the four points labelled in figure 2. In order to maximize the inelastic contribution to the signal, ω_1 (ω_2) is set 8 eV to the red (blue) of the pulse central frequency. The interpulse delay is taken to be $T = 0$ in these plots.

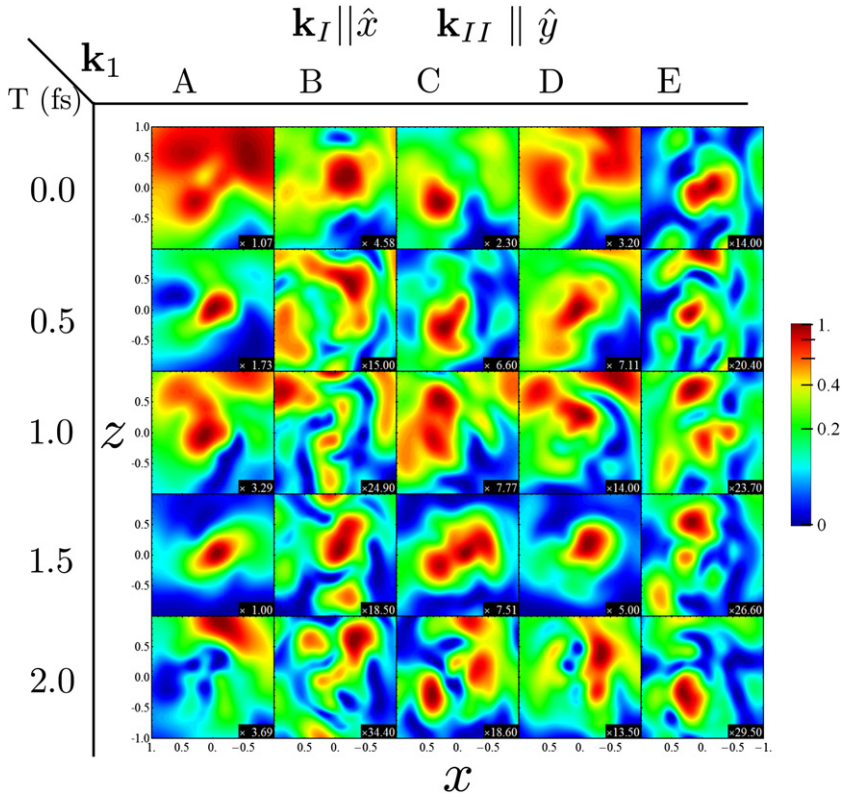

Figure 6. Same as figure 5 but with $\mathbf{k}_{II}$ set to the lab-frame y-axis.

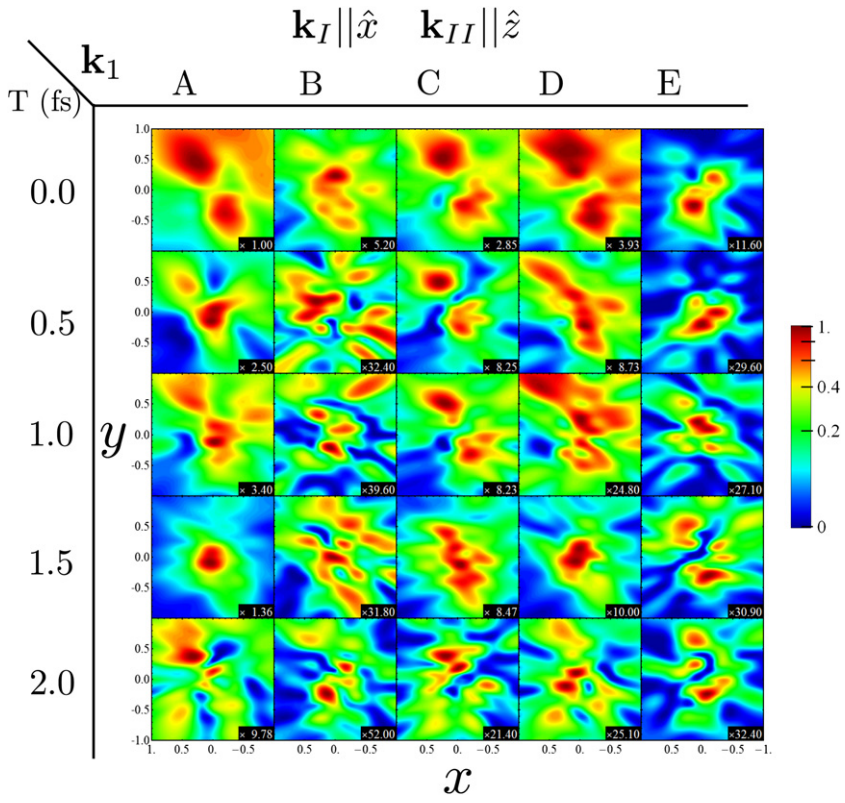

Figure 7. Same as figure 5 but with $\mathbf{k}_{II}$ set to the lab-frame z-axis.

choose a projection of the total superposition created by the scattering event. The bottom rows of figure 5 show that the $\mathbf{k}_2$ scattering pattern depends on time as well as on $\mathbf{k}_1$.

Figures 6 and 7 show the $\mathbf{k}_2$ scattering pattern when the second pulse wavevector $\mathbf{k}_{II}$ is parallel to the y- and z-axis, respectively. We can see that the particular superposition state for $\mathbf{k}_1$ peaks A and D are very similar initially, but become different as the delay time increases.

4. Conclusions

We have proposed a new type of measurement that uses scattered off-resonant x-ray light to probe multipoint correlation functions of the charge density. This signal involves the coincident measurement of two or more photons, with control over the timing and wavevector for both, which represents an extreme experimental challenge. The times T_1 and T_2 are controlled by the incoming pulses. To control $\mathbf{k}_1$ and $\mathbf{k}_2$ we must work at low fluxes where single-photon coincidence counting is possible. At high fluxes the correlation information carried by the wavevectors will be eroded.

Simulations presented for the amino acid cysteine show that these signals are highly dependent on the time-evolving charge density. Static contributions resulting from diagonal elements of the charge density, can be eliminated from the scattering signal by setting the detection frequency outside the pulse bandwidth. Additional information is available through these measurements than in traditional x-ray diffraction, which solely depends on diagonal elements of the charge-density operator.

Acknowledgments

The support of the Chemical Sciences, Geosciences, and Biosciences division, Office of Basic Energy Sciences, Office of Science, US Department of Energy is gratefully acknowledged. YZ and KB were supported by the DOE. We also gratefully acknowledge the support of the National Science Foundation (grants CHE-1058791 and CHE-0840513), and the National Institutes of Health (grant GM-59230).

References

[1] Glover T *et al* 2012 X-ray and optical wave mixing *Nature* **488** 603–8
[2] Bucksbaum P H 2007 The future of attosecond spectroscopy *Science* **317** 766–9
[3] Krausz F and Ivanov M 2009 Attosecond physics *Rev. Mod. Phys.* **81** 163
[4] Popmintchev T, Chen M-C, Arpin P, Murnane M M and Kapteyn H C 2010 The attosecond nonlinear optics of bright coherent x-ray generation *Nature Photon.* **4** 822–32
[5] Gallmann L, Cirelli C and Keller U 2012 Attosecond science: recent highlights and future trends *Annu. Rev. Phys. Chem.* **63** 447–69
[6] Ullrich J, Rudenko A and Moshammer R 2012 Free-electron lasers: new avenues in molecular physics and photochemistry *Annu. Rev. Phys. Chem.* **63** 635–60
[7] Mukamel S, Healion D, Zhang Y and Biggs J D 2013 Multidimensional attosecond resonant x-ray spectroscopy of molecules: lessons from the optical regime *Annu. Rev. Phys. Chem.* **64** 101–27

[8] Rahav S and Mukamel S 2010 Multidimensional attosecond photoelectron spectroscopy with shaped pulses and quantum optical fields *Phys. Rev.* A **81** 063810
[9] Biggs J D, Zhang Y, Healion D and Mukamel S 2013 Watching energy transfer in metalloporphyrin heterodimers using stimulated x-ray Raman spectroscopy *Proc. Natl Acad. Sci.* **110** 15597–601
[10] Chapman H N, Fromme P, Barty A, White T A, Kirian R A, Aquila A, Hunter M S, Schulz J, DePonte D P and Weierstall U 2011 Femtosecond x-ray protein nanocrystallography *Nature* **470** 73–7
[11] Koopmann R *et al* 2012 *In vivo* protein crystallization opens new routes in structural biology *Nature Methods* **9** 259–62
[12] Dorfman K E, Bennett K, Zhang Y and Mukamel S 2013 Nonlinear light scattering in molecules triggered by an impulsive x-ray Raman process *Phys. Rev.* A **87** 053826
[13] Tanaka S, Chernyak V and Mukamel S 2001 Time-resolved x-ray spectroscopies: nonlinear response functions and Liouville-space pathways *Phys. Rev.* A **63** 063405
[14] Dixit G, Vendrell O and Santra R 2012 Imaging electronic quantum motion with light *Proc. Natl Acad. Sci.* **109** 11636–40
[15] Bennett K, Biggs J D, Zhang Y, Dorfman K E and Mukamel S 2013 Time, frequency, and wavevector resolved x-ray diffraction from single molecules *Nature Commun.* submitted
[16] Freyer B, Zamponi F, Juvé V, Stingl J, Woerner M, Elsaesser T and Chergui M 2013 Ultrafast inter-ionic charge transfer of transition-metal complexes mapped by femtosecond x-ray powder diffraction *J. Chem. Phys.* **138** 144504
[17] Bargheer M, Zhavoronkov N, Gritsai Y, Woo J C, Kim D S, Woerner M and Elsaesser T 2004 Coherent atomic motions in a nanostructure studied by femtosecond x-ray diffraction *Science* **306** 1771–3
[18] Stingl J, Zamponi F, Freyer B, Woerner M, Elsaesser T and Borgschulte A 2012 Electron transfer in a virtual quantum state of $LiBH_4$ induced by strong optical fields and mapped by femtosecond x-ray diffraction *Phys. Rev. Lett.* **109** 147402
[19] Vrakking M J J and Elsaesser T 2012 X-ray photonics: x-rays inspire electron movies *Nature Photon.* **6** 645–7
[20] Mukamel S 1995 *Principles of Nonlinear Optical Spectroscopy* 1st edn (New York: Oxford University Press)
[21] Healion D, Biggs J D and Mukamel S 2012 Manipulating one- and two-dimensional stimulated-x-ray resonant-Raman signals in molecules by pulse polarizations *Phys. Rev.* A **86** 033429
[22] Biggs J D, Zhang Y, Healion D and Mukamel S 2013 Multidimensional x-ray spectroscopy of valence and core excitations in cysteine *J. Chem. Phys.* **138** 144303
[23] Murnane M M and Miao J 2009 Optics: ultrafast x-ray photography *Nature* **460** 1088–90
[24] Barty A 2010 Time-resolved imaging using x-ray free electron lasers *J. Phys. B: At. Mol. Opt. Phys.* **43** 194014
[25] Rivière P, Palacios A, Pérez-Torres J F and Martín F 2012 Probing electron dynamics in simple molecules with attosecond pulses *Progress in Ultrafast Intense Laser Science VIII* (Berlin: Springer) pp 1–28
[26] Dwyer J R, Hebeisen C T, Ernstorfer R, Harb M, Deyirmenjian V B, Jordan R E and Miller R D 2006 Femtosecond electron diffraction: making the molecular movie *Phil. Trans. R. Soc.* A **364** 741–78
[27] Biggs J D, Voll J A and Mukamel S 2012 Coherent nonlinear optical studies of elementary processes in biological complexes; diagrammatic techniques based on the wavefunction versus the density matrix *Phil. Trans. R. Soc.* A **370** 3709–27
[28] Zhang Y, Biggs J D, Healion D, Govind N and Mukamel S 2012 Core and valence excitations in resonant x-ray spectroscopy using restricted excitation window time-dependent density functional theory *J. Chem. Phys.* **137** 194306
[29] Frisch M J *et al* 2009 *Gaussian 09* (Wallingford, CT: Gaussian Inc.)
[30] Becke A D 1993 Density-functional thermochemistry: III. The role of exact exchange *J. Chem. Phys.* **98** 5648
[31] Stephens P J, Devlin F J, Chabalowski C F and Frisch M J 1994 *Ab initio* calculation of vibrational absorption and circular dichroism spectra using density functional force fields *J. Phys. Chem.* **98** 11623–7
[32] Yanai T, Tew D and Handy N 2004 A new hybrid exchangecorrelation functional using the coulomb-attenuating method (CAM-B3LYP) *Chem. Phys. Lett.* **393** 51
[33] Hirata S and Head-Gordon M 1999 Time-dependent density functional theory within the Tamm–Dancoff approximation *Chem. Phys. Lett.* **314** 291
[34] Valiev M *et al* 2010 NWChem: a comprehensive and scalable open-source solution for large scale molecular simulations *Comput. Phys. Commun.* **181** 1477–89
[35] Lopata K, Van Kuiken B E, Khalil M and Govind N 2012 Linear-response and real-time time-dependent density functional theory studies of core-level near-edge x-ray absorption *J. Chem. Theory Comput.* **8** 3284–92
[36] Handy N C and Schaefer H F 1984 On the evaluation of analytic energy derivatives for correlated wave functions *J. Chem. Phys.* **81** 5031–3
[37] Yamaguchi Y, Osamura Y, Goddard J D and Schaefer H F 1994 *A New Dimension to Quantum Chemistry: Analytic Derivative Methods in Ab Initio Molecular Electronic Structure Theory* (New York: Oxford University Press)